Hindawi
Geofluids
Volume 2022, Article ID 1302260, 12 pages
https://doi.org/10.1155/2022/1302260

Research Article

Theoretical Research on Grouting in Deep Loose Layers Based on the Cylindrical Diffusion Model of Radial Tube Flow

Xuesong Wang,[1] **Hua Cheng**,[1,2,3] **Zhishu Yao**,[1] **Chuanxin Rong**,[1] **Xianwen Huang**,[1] **and Longhui Guo**[1]

[1]*School of Civil Engineering and Architecture, Anhui University of Science and Technology, Huainan, Anhui 232001, China*
[2]*School of Resources and Environmental Engineering, Anhui University, Hefei, Anhui 230601, China*
[3]*Anhui Province Key Laboratory of Building Structure and Underground Engineering, Anhui Jianzhu University, Hefei, Anhui 230601, China*

Correspondence should be addressed to Hua Cheng; hcheng@aust.edu.cn

Received 19 January 2022; Revised 25 February 2022; Accepted 2 March 2022; Published 25 March 2022

Academic Editor: Xueming Du

Grouting in deep, loose layers are a complex process in which many modes such as infiltration, splitting, and compaction coexist. It is of great significance to establish a realistic, simplified physical model to study the law of slurry diffusion. Herein, a cylindrical diffusion model of radial tube flow is established, and the control differential equations of both the Bingham slurry diffusion velocity in a single tube and the diffusion velocity of the radial tube flow are deduced. Additionally, the calculation formulas for the diffusion radius and slurry pressure distribution function are obtained. The rationality of the theory is verified by combining our results with those of the field grouting test of the Guotun coal mine. The results show that the cylindrical diffusion model of radial tube flow can successfully characterize the slurry diffusion law of grouting in a deep, loose layer. The slurry pressure attenuation shows distinguishable stages: within the first 30% of the diffusion radius, the slurry pressure decreased sharply by approximately 70%, and the slurry pressure decreases slowly in the later stages. Furthermore, the diffusion radius has a nonlinear, negative correlation with the height of the grouting section and the comprehensive injection rate of formation; the change rate is relatively more gradual, and there are no distinguishable stages. The research results provide a theoretical basis for reasonably determining the grouting parameters of deep, loose layers in the future.

1. Introduction

As a common treatment method for antiseepage, plugging, and reinforcement of underground engineering, grouting methods are widely used in mine water plugging and reinforcement, water and mud inrush treatment in tunnel fault fracture zones, foundation pit supports, dam reinforcement, and other fields [1–3]. Grouting in deep and loose layers has the typical "three high characteristics" of high ground stress, high permeability, and high grouting pressure [4, 5]. In addition, the uncertainty of the change in soil layer properties during the deposition process leads to many modes of slurry diffusion, such as splitting, permeability, and compaction, and its diffusion mechanism and design theory have significantly lag between engineering practice and research [6, 7].

Regarding the diffusion of split grouting slurry, the main established mathematical models include the flat-plate diffusion model that does not consider the change in crack width and the plane radiation circle diffusion model that does consider the change in crack width [8–10]. The main research topics are slurry diffusion radius and velocity distribution, pressure distribution, and viscosity temporal and spatial distribution in the process of migration. Regarding infiltration grouting, numerous studies have been conducted with a combination of different flow patterns of slurry and different diffusion models. The slurry flow patterns of Newtonian, Bingham, and power-law fluids have been investigated. The established diffusion models mainly include the spherical, cylindrical, and cylindrical-hemispherical models [11–14]. Regarding compaction grouting, the fluid–solid coupling

effect between the slurry and soil is mainly studied in combination with the theories of ball hole expansion or column hole expansion and soil nonlinear compaction. The research focus is mainly on considering different yield criteria, dilatancy, strain softening, different moduli of tension, and compression of soil [15–17].

The above researches ignored the tortuous effect in the process of slurry diffusion and assumed that the diffusion channels of slurry were straight. There was a large deviation between the theoretical calculation results and the engineering practice. Through comparison, some scholars [18–20] have found that the slurry diffusion law considering the tortuous effect was more consistent with the grouting test results, and the calculation error was smaller. It is of great significance to consider the tortuous effect in the design of grouting parameters in porous media. In addition, the abovementioned research only discusses a particular diffusion mode of the slurry, but the process of grouting in deep, loose layers involves multiple diffusion modes [21, 22]. The grouting theory of the single diffusion mode cannot be applied when designing the grouting parameters in deep, loose layers. The grouting construction parameter design is not significantly influenced by the slurry diffusion mode but focuses on the design of parameters such as grouting pressure and diffusion radius [23, 24]. Therefore, it is necessary to establish a grouting diffusion theory suitable for deep, loose layers, which simultaneously weakens the slurry diffusion mode and can be better suited to guide the design of grouting parameters.

Grotenhuis et al. [25, 26] characterized the slurry diffusion channel in sand with a straight circular tube and assumed the diffusion of the slurry in the sand to be represented by the flow of the slurry in the circular tube. The model can characterize both the split grouting and infiltration grouting mechanisms and can be used to calculate parameters such as the grouting pressure and diffusion radius. Based on this and considering the tortuous effect of the slurry diffusion path, this study considers the slurry diffusion channel in sand to be a tortuous circular tube and establishes the cylindrical diffusion model of the radial tube flow of the slurry in a deep, loose sand layer. First, the control differential equation of the Bingham slurry diffusion velocity in a single tube is derived, and the permeability coefficient considering tortuosity is used to replace the average radius of the seepage tubes in the injected layer within the differential equation. Subsequently, the diffusion velocity control equation of the radiation tube flow is derived, and the calculation formulas for the diffusion radius and slurry pressure distribution function are obtained. Finally, combined with the field grouting test results of the Guotun coal mine, the rationality of the theory is verified, and the attenuation law of the grouting pressure and the influential factors on the diffusion radius are discussed for the diffusion area. The research results provide a reference for future guidance of the design of grouting parameters in deep and loose layers.

2. Cylindrical Diffusion Model of Radial Tube Flow

2.1. Basic Assumptions and Model Establishment. To simplify the calculation and establish the diffusion model of the slurry in a deep, loose sand layer, the following assumptions are made within this study:

(1) The diffusion mode of the slurry in the layer is weakened, and the diffusion of slurry in splitting cracks and pores is regarded as the flow of slurry in tortuous tubes

(2) The slurry is an incompressible Bingham fluid, and the slurry flow pattern does not change during grouting

(3) The slurry velocity on the inner wall of the tube is 0, which satisfies the no-slip boundary condition

(4) The energy loss of the slurry flowing through the bend of the tube was ignored

Based on the abovementioned assumptions, a cylindrical diffusion model of the radial tube flow of the slurry in a deep, loose sandy soil layer is constructed, where the height of the grouting section is h, and the diffusion radius is R. N horizontal circuitous circular tubes with radius r_0 radiate from the vicinity of the grouting tube, where r_0 is the comprehensive average radius of the tubes, and the diffusion of the slurry in the sand layer is regarded as the flow of the slurry in circuitous circular tubes. The specific values of N and r_0 of the tubes are difficult to determine, but it is possible to simplify the theoretical derivation process by eliminating these two parameters. Therefore, a cylindrical surface coaxial within the grouting tube is selected, where the height of the cylindrical surface is equal to the height h of the grouting section ,and the radius is set to R_0, which satisfies the following requirement:

$$N\pi r_0^2 = 2\pi R_0 h. \tag{1}$$

It is worth noting that R_0 is neither the grouting tube radius nor the drilling radius. This cylindrical surface is an imaginary cylindrical surface selected for the convenience of the subsequent theoretical derivation, which is referred to as the virtual divergent surface in this study. According to Equation (1), the sum of the cross-sectional areas of all tubes is equal to the side surface area of the divergence surface, which is equivalent to the radial divergence of the slurry from the virtual divergence surface within the tortuous circular tube. A schematic of the diffusion model is shown in Figure 1.

2.2. Diffusion Velocity Control Differential Equation of Bingham Slurry in a Single Tube. The Bingham fluid rheological equation is as follows [27]:

$$\tau = \tau_0 + \eta_g \dot{\gamma}, \tag{2}$$

where τ is the shear stress between grout layers, τ_0 is the shear yield strength of the slurry, η_g is the viscosity coefficient of the slurry at 25°C, and $\dot{\gamma} = -\mathrm{d}v/\mathrm{d}\rho$ is the shear rate of the slurry.

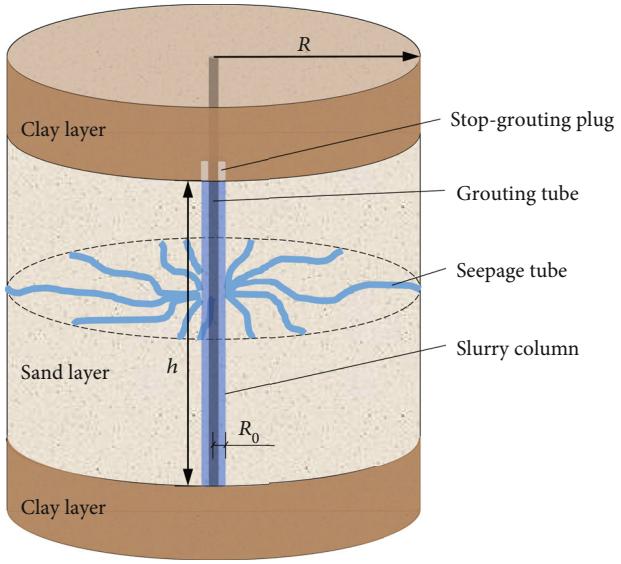

Figure 1: Cylindrical diffusion model of radial tube flow.

The actual length of the tortuous circular tube is $\chi(R - R_0)$, the radius is r_0, the slurry pressure upon entry is the initial grouting pressure, and the slurry pressure at the end is the hydrostatic pressure p_w at this point. The x-axis of the natural coordinate system along the axis of the tortuous circular tube is established, and the intersection of the x-axis and the grouting tube axis is taken as the coordinate origin. The slurry flow direction is along the positive x-axis. $[0, R_0]$ is the straight-line section, and $[R_0, \chi(R - R_0) + R_0]$ is the tortuous section, as shown in Figure 2(a). The attenuation value of the slurry pressure along the x-axis was set as $p(x)$. Note that the value of $p(x)$ represents the attenuation value of the slurry pressure, which is therefore distinguished from the slurry pressure. The boundary conditions are

$$\begin{cases} x = R_0, p = 0, \\ x = \chi(R - R_0) + R_0, p = p_0 - p_w. \end{cases} \tag{3}$$

A section of the cylindrical fluid microelement with radius ρ and length dx and its axial force is shown in Figure 2(b), which is obtained from the equilibrium conditions of the axial force:

$$\{[p_0 - p(x + dx)] - [p_0 - p(x)]\} \cdot \pi\rho^2 + \tau \cdot 2\pi\rho \cdot dx = 0, \tag{4}$$

which can be simplified to

$$p(x + dx) - p(x) = \frac{2\tau}{\rho} dx. \tag{5}$$

Let $dp = p(x + dx) - p(x)$, and then Equation (5) can be simplified to

$$dp = \frac{2\tau}{\rho} dx. \tag{6}$$

Therefore, along the slurry flow direction, the pressure attenuation gradient can be expressed as follows:

$$\lambda = \frac{dp}{dx} = \frac{2\tau}{\rho}. \tag{7}$$

The pressure attenuation gradient, λ, is the attenuation speed of the pressure along the flow direction. It can be seen from Equation (7) that λ is positively correlated with the slurry shear stress, τ, and negatively correlated with radial distance, ρ. τ is positively correlated with the slurry viscosity. The greater the viscosity, the more difficult it is to overcome the shear stress, the greater τ is, and the faster the pressure attenuation is. When the radial distance ρ is equal to the tube radius r_0, the average starting pressure gradient of the slurry flowing in the tube is

$$\lambda_0 = \frac{2\tau_0}{r_0}, \tag{8}$$

where λ_0 is the average starting pressure gradient of the slurry, τ_0 is the shear yield strength of the slurry, and r_0 is the comprehensive average radius of the tubes, which is positively correlated with the effective porosity of sand, and is the parameter after homogenizing the pore channel size of sand. According to [28], the calculation formula for r_0 is

$$r_0 = \frac{\sum_{i=1}^{n} N_i r_i^4}{\sum_{i=1}^{n} N_i r_i^3} \approx \left(\frac{\sum_{i=1}^{n} N_i r_i^4}{\sum_{i=1}^{n} N_i}\right)^{\frac{1}{4}}, \tag{9}$$

where N_i is the number of tubes with a cross-section radius of r_i $(i = 1, 2, \cdots, n)$.

From Equation (7), it is then possible to obtain the following:

$$\tau = \frac{\rho}{2} \cdot \frac{dp}{dx}. \tag{10}$$

Substituting Equation (10) into Equation (2) results in

$$-\frac{dv}{d\rho} = \frac{1}{\eta_g}\left(\frac{\rho}{2} \cdot \frac{dp}{dx} - \tau_0\right). \tag{11}$$

When $\tau \le \tau_0$, the slurry moves as a piston, $dv/d\rho = 0$, with a radius of r_p and a speed of v_p. Using Equation (11), we obtain

$$r_p = \frac{2\tau_0}{dp/dx}. \tag{12}$$

When $\tau > \tau_0$, the slurry moves in a laminar flow. From Equation (11), we can separate the variables and integrate, resulting in

$$v = -\frac{1}{\eta_g}\left(\frac{\rho^2}{4} \cdot \frac{dp}{dx} - \tau_0\rho\right) + C_1, \tag{13}$$

where C_1 is the integration constant.

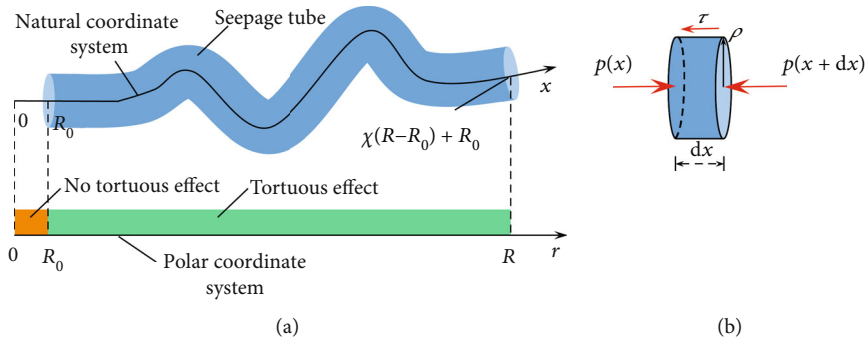

Figure 2: Coordinate system and fluid microelement stress diagram.

Substituting the no-slip boundary condition, i.e., $\rho = r_0$, the integration constant is determined to be

$$C_1 = \frac{1}{\eta_g}\left(\frac{r_0^2}{4}\cdot\frac{dp}{dx} - \tau_0 r_0\right). \tag{14}$$

Therefore, the velocity distribution of the laminar flow in $[r_p, r_0]$ is

$$v = \frac{1}{\eta_g}\left[\frac{r_0^2-\rho^2}{4}\cdot\frac{dp}{dx} - \tau_0(r_0-\rho)\right], \tag{15}$$

and the fluid velocity of the piston-like flow in $[0, r_p]$ is

$$v_p = \frac{1}{\eta_g}\left[\frac{r_0^2-r_p^2}{4}\cdot\frac{dp}{dx} - \tau_0(r_0-r_p)\right]. \tag{16}$$

The velocity distribution in the circular tube is a truncated paraboloid shape, and the flow rate per unit time, q_1, in a single tube is

$$q_1 = \pi r_p^2 v_p + \int_{r_p}^{r_0} 2\pi\rho v d\rho. \tag{17}$$

Substituting Equations (15) and (16) into Equation (17), we obtain

$$q_1 = \frac{\pi r_0^4}{8\eta_g}\cdot\frac{dp}{dx}\cdot\left[1 - \frac{4}{3}\left(\frac{r_p}{r_0}\right) + \frac{1}{3}\left(\frac{r_p}{r_0}\right)^4\right]. \tag{18}$$

The average velocity, $\bar{v}$, within the tube section is

$$\bar{v} = \frac{r_0^2}{8\eta_g}\cdot\frac{dp}{dx}\cdot\left[1 - \frac{4}{3}\left(\frac{r_p}{r_0}\right) + \frac{1}{3}\left(\frac{r_p}{r_0}\right)^4\right]. \tag{19}$$

Substituting Equation (12) into Equation (19) results in

$$\bar{v} = \frac{r_0^2}{8\eta_g}\cdot\frac{dp}{dx}\cdot\left[1 - \frac{4}{3}\left(\frac{2\tau_0/r_0}{dp/dx}\right) + \frac{1}{3}\left(\frac{2\tau_0/r_0}{dp/dx}\right)^4\right]. \tag{20}$$

From Equation (20), it can be seen that when $2\tau_0/r_0/dp/dx = 1$, $\bar{v} = 0$. Specifically, when the pressure gradient $\lambda = 2\tau_0/r_0 = \lambda_0$, the average flow in the circular tube is 0.

To satisfy $dp/dx = \lambda_0$ and $\bar{v} = 0$, Equation (20) is rewritten as

$$\bar{v} = \frac{r_0^2}{8\eta_g}\cdot\frac{dp}{dx}\cdot\left\{1 - \frac{\lambda_0}{dp/dx} - \frac{1}{3}\cdot\frac{\lambda_0}{dp/dx}\cdot\left[1 - \left(\frac{\lambda_0}{dp/dx}\right)^3\right]\right\}. \tag{21}$$

In the grouting process, $dp/dx \gg \lambda_0$ [28], the third term in the curly bracket of Equation (21) is ignored in order to obtain an approximate slurry diffusion velocity control differential equation, as follows:

$$\bar{v} = \frac{r_0^2}{8\eta_g}\cdot\left(\frac{dp}{dx} - \lambda_0\right). \tag{22}$$

Owing to the uneven spatial distribution of the pore structure in the injected layer, the average radius, r_0, of the seepage tube in the injected layer in Equation (22) is difficult to measure directly. However, the permeability coefficient can be easily obtained through laboratory tests. Therefore, the expression of the permeability coefficient was used to replace r_0 within this study. The relationship between the permeability coefficient and r_0 is derived as follows:

The relationship between the permeability coefficient K and permeability k is [29]

$$K = k\frac{\gamma}{\eta}, \tag{23}$$

where γ is the gravity of the fluid, and η is the viscosity coefficient of the fluid.

The permeability of porous media is independent of the fluid characteristics and only depends on the porosity, capillary diameter, and tortuosity of the porous media. The existing theory only uses porosity and capillary diameter to characterize the permeability of porous media, without considering the nonnegligible parameter of tortuosity [28]. It is worth noting that because permeability is independent of the fluid characteristics, to simplify the calculation, the fluid

selected in the process of deriving permeability is the laminar Newtonian fluid, which does not conflict with the Bingham fluid studied within this research.

According to the generalized Hagen Poiseuille equation [30], the flow through all tubes per unit time is

$$q = \frac{nA\pi r_0^4}{8\eta\chi} \cdot \frac{\mathrm{d}p}{\mathrm{d}l}, \tag{24}$$

where q is the flow through the pore section, n is the number of circular tubes per unit area, A is the cross-sectional area, and $\mathrm{d}p/\mathrm{d}l$ is the pressure gradient.

In the laminar flow state, the flow of fluid in porous media satisfies Darcy's law, and the flow through the pore section per unit time is

$$q = \frac{kA}{\eta} \cdot \frac{\mathrm{d}p}{\mathrm{d}l}. \tag{25}$$

Through theoretical derivation, Li et al. [31] highlighted how the tube flow and seepage flow are unified, and the formulas of the two mathematical models are equivalent; they are simply expressed by different parameters. In combination with Equations (24) and (25), the permeability considering tortuosity is

$$k = \frac{n\pi r_0^4}{8\chi}. \tag{26}$$

The porosity of the tube model is

$$\varphi = n\pi r_0^2 \chi. \tag{27}$$

When combining Equations (26) and (27), we find

$$k = \frac{\varphi r_0^2}{8\chi^2}. \tag{28}$$

Therefore, the permeability coefficient considering tortuosity is

$$K = \frac{\varphi r_0^2 \gamma}{8\eta\chi^2}. \tag{29}$$

Setting the viscosity ratio of slurry to water to β, we obtain

$$\beta = \frac{\eta_g}{\eta_w}, \tag{30}$$

where η_w is the viscosity coefficient of water at 25°C.

Combining Equations (29) and (30) results in

$$\frac{r_0^2}{8\eta} = \frac{\chi^2 K_w}{\beta\varphi\gamma_w}, \tag{31}$$

where K_w is the permeability coefficient of water in a porous medium.

Therefore, Equation (22) can be transformed into

$$\bar{v} = \frac{\chi^2 K_w}{\beta\varphi\gamma_w} \cdot \left(\frac{\mathrm{d}p}{\mathrm{d}x} - \lambda_0\right). \tag{32}$$

Equation (32) is the approximate slurry diffusion velocity control differential equation of the Bingham slurry in a single tube.

2.3. Diffusion Velocity Control Equation of Radial Tube Flow. The flow and diffusion path of the slurry in the deep, loose layer was tortuous, as shown in Figure 3. Tortuosity is used to characterize the tortuous effect of fluid particle motion diffusion [32, 33], which is commonly defined as

$$\chi = \frac{l_t}{l}, \tag{33}$$

where χ is the tortuosity of the tube which commonly takes the values obtained by related scholars of 1.4 ~ 1.6 [28]. The average value used within this research is 1.5, l_t is the actual length of the diffusion trace, and l is the effective length of the diffusion path.

The effective porosity of the injected layer is the ratio of the pore volume filled by the slurry to the volume of the injected soil layer, and the relationship with the porosity of the soil layer is

$$\varphi' = \alpha\varphi, \tag{34}$$

where φ' is the effective porosity of the injected layer, φ is the actual porosity of the injected layer, and α is the pore injection coefficient of approximately 0.15~0.2 for silty clay and 0.3 ~ 0.5 for soft soil and fine sand [34].

In the hollow cylindrical layer of $[R_0, (x - R_0)/\chi + R_0]$, the effective porosity is

$$\varphi' = \frac{N\pi r_0^2 (x - R_0)}{\pi h\left\{\left[(x - R_0)/\chi + R_0\right]^2 - R_0^2\right\}}. \tag{35}$$

Combining Equations (1) and (35) results in

$$\varphi' = \frac{2\chi^2 R_0}{x + (2\chi - 1)R_0}. \tag{36}$$

It can be seen from Equation (36) that the effective porosity decreases with an increase in the diffusion distance, which is consistent with practice. An increase in the slurry diffusion distance means that the slurry pressure gradient gradually decreases. When it is less than the starting pressure gradient of the slurry flow in small tubes, the slurry will not enter these small tubes. When the distance from the grouting tube increases, the number of pores that the slurry can enter gradually decreases; that is, the effective porosity gradually decreases.

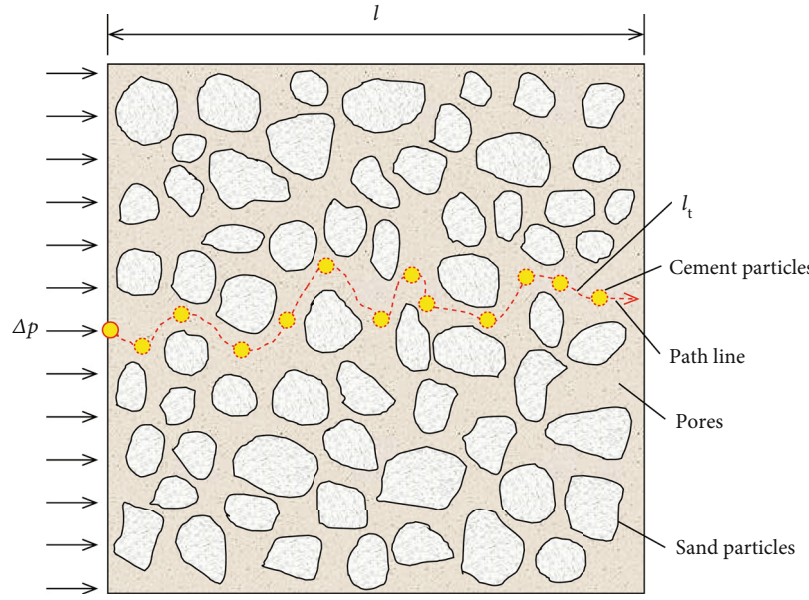

Figure 3: Schematic of slurry diffusion tortuous effect.

The slurry column radius can be obtained by combining Equations (34) and (36), such that

$$R_0 = \frac{\alpha\varphi}{2\chi^2 - (2\chi - 1)\alpha\varphi}x. \tag{37}$$

It can be seen from Equation (37) that during grouting, the slurry column radius changes with the change in effective porosity and diffusion distance, which is not a fixed value.

Let

$$\xi = \frac{\alpha\varphi}{2\chi^2 - (2\chi - 1)\alpha\varphi}, \tag{38}$$

where ξ is a parameter selected to simplify the formula, which is related to α, φ, and χ, and is calculated by Equation (38).

Then,

$$R_0 = \xi x. \tag{39}$$

Because the slurry is incompressible, the slurry injection flow is equal to the outflow flow of the cylindrical surface outside the slurry column,

$$q = \frac{\bar{v}}{\chi} \cdot 2\pi R_0 h. \tag{40}$$

Combining Equations (39) and (40) results in

$$\bar{v} = \frac{\chi q}{2\pi\xi h x}. \tag{41}$$

2.4. Slurry Diffusion Radius and Pressure Distribution. Through combining Equations (32) and (41), we obtain

$$\frac{\mathrm{d}p}{\mathrm{d}x} = \frac{q\beta\varphi\gamma_w}{2\pi\xi h\chi K_w}\frac{1}{x} + \lambda_0. \tag{42}$$

Subsequently, integrating Equation (42) results in

$$p(x) = \frac{q\beta\varphi\gamma_w}{2\pi\xi h\chi K_w}\ln x + \lambda_0 x + C. \tag{43}$$

When the following boundary conditions are implemented, we have

$$x = R_0, p = 0. \tag{44}$$

The integration constant is determined to be

$$C = -\frac{q\beta\varphi\gamma_w}{2\pi\xi h\chi K_w}\ln R_0 - \lambda_0 R_0 \tag{45}$$

By substituting Equation (45) into Equation (43), we obtain

$$p(x) = \frac{q\beta\varphi\gamma_w}{2\pi\xi h\chi K_w}\ln\frac{x}{R_0} + \lambda_0(x - R_0). \tag{46}$$

Equation (46) describes the relationship between the pressure attenuation value and the path distance of the diffusion curve. Three transformations are required to transform this into the relationship between the pressure attenuation value and diffusion distance. First, the function image is shifted to the right by the a factor ofR_0. Then, the ordinate of the function is unchanged, and the abscissa becomes $1/\chi$ the original. Finally, the function image is shifted to the left by a factor of R_0. The transformed function is $p(\chi(x - R_0)$

$+R_0$), and to clarify the difference, the abscissa of the new function is represented by the letter r, representing the slurry diffusion distance, and the ordinate is represented by $\tilde{p}$, representing the slurry pressure attenuation value at the diffusion distance R. Then, the relationship between the pressure attenuation value and the diffusion distance is

$$\tilde{p}(r) = \frac{q\beta\varphi\gamma_w}{2\pi\xi h\chi K_w} \ln \frac{\chi(r-R_0)+R_0}{R_0} + \lambda_0\chi(r-R_0). \quad (47)$$

The pressure attenuation value at the diffusion radius R is

$$\tilde{p}(R) = \frac{q\beta\varphi\gamma_w}{2\pi\xi h\chi K_w} \ln \frac{\chi(R-R_0)+R_0}{R_0} + \lambda_0\chi(R-R_0). \quad (48)$$

Therefore, the initial grouting pressure is

$$p_0 = p_w + \frac{q\beta\varphi\gamma_w}{2\pi\xi h\chi K_w} \ln \frac{\chi(R-R_0)+R_0}{R_0} + \lambda_0\chi(R-R_0). \quad (49)$$

The slurry pressure distribution function, $P(r)$, in the diffusion area is

$$P(r) = p_0 - \tilde{p}(r) = p_w + \frac{q\beta\varphi\gamma_w}{2\pi\xi h\chi K_w} \ln \frac{\chi(R-R_0)+R_0}{\chi(r-R_0)+R_0} + \lambda_0\chi(R-r). \quad (50)$$

However, the grouting diffusion radius, R, is usually unknown, and its calculation formula needs to be deduced. According to Equation (41), when the diffusion radius is R, the slurry column radius is

$$R_0 = \xi R. \quad (51)$$

The volume of the slurry filled in the layer is equal to the total amount of slurry injected, such that

$$\alpha\varphi\pi\left(R^2 - R_0^2\right)h + \pi R_0^2 h = Q. \quad (52)$$

Namely,

$$\left[\xi^2 + \alpha\varphi\left(1-\xi^2\right)\right]\pi R^2 h = Q. \quad (53)$$

Let

$$\eta = \xi^2 + \alpha\varphi\left(1-\xi^2\right), \quad (54)$$

where η is the comprehensive injection rate of the layer.

The grouting diffusion radius can be calculated according to the grouting volume, grouting section height, and comprehensive injection rate of the layer as follows:

$$R = \sqrt{\frac{Q}{\pi h\eta}}. \quad (55)$$

Therefore, the initial grouting pressure is

$$p_0 = p_w + \frac{q\beta\varphi\gamma_w}{2\pi\xi h\chi K_w} \ln \frac{\chi\left(\sqrt{Q/\pi h\eta} - R_0\right) + R_0}{R_0} + \lambda_0\chi\left(\sqrt{\frac{Q}{\pi h\eta}} - R_0\right), \quad (56)$$

and the slurry pressure distribution function, $P(r)$, in the diffusion area is

$$P(r) = p_w + \frac{q\beta\varphi\gamma_w}{2\pi\xi h\chi K_w} \ln \frac{\chi\left(\sqrt{Q/\pi h\eta} - R_0\right) + R_0}{\chi(r-R_0)+R_0} + \lambda_0\chi\left(\sqrt{\frac{Q}{\pi h\eta}} - r\right). \quad (57)$$

3. Results and Discussion

3.1. Field Test Verification and Analysis. To verify the applicability of the cylindrical diffusion model of radial tube flow established in this study, we compared the theoretical calculations with the field test results of ground drilling grouting in the Guotun coal mine. The main, auxiliary, and air shafts of the Guotun coal mine in Shandong Province pass through the loose layer with a thickness of 561.20~587.40 m. After the mine was put into operation, owing to the drainage of the mine, the above three shafts deviated to the asymmetric mining working face of the mine. The maximum deflection displacements of the main shaft and auxiliary shaft to the west were 284 mm and 299 mm, respectively, and the maximum deflection displacements to the north were 30 mm and 103 mm, respectively, which seriously threaten the production safety of the mine. After many demonstrations, it was decided to adopt the scheme of ground drilling grouting around the shaft to control the shaft deflection displacements. The engineering site diagram and schematic diagram of the ground drilling grouting of the vertical shaft are shown in Figure 4. To scientifically formulate the grouting implementation scheme, reasonably select the grouting parameters, and to ensure the safety of the existing shaft, 11 water injection tests and 6 grouting tests were completed in different layers in 7 test holes around the main, auxiliary, and air shafts of the Guotun coal mine. 5 grouting tests were conducted on the water-bearing sand layers over different layers of the loose layer within the 3rd wind inspection hole.

Single cement slurry was used for grouting. The main grouting material is 42.5 ordinary portland cement, which is prepared by adding water to the cement. The water

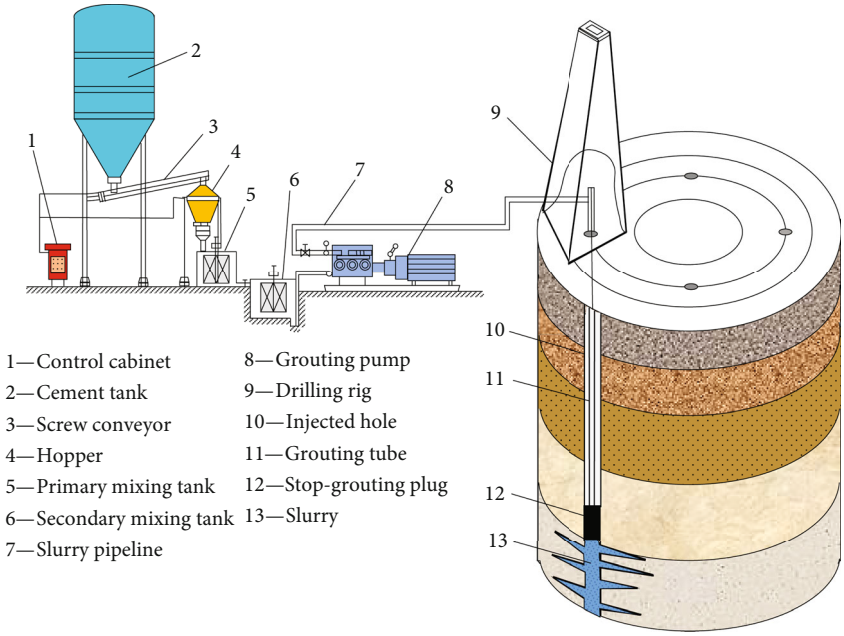

Figure 4: Vertical shaft ground drilling grouting.

Table 1: Physical parameters of the core soil samples taken from the 3rd wind inspection hole.

Soil sample no.	Soil sample type	h (m)	φ	K
01	Fine sand	180.60~180.75	0.3106	1.138
02	Silty sand	281.20~281.35	0.3333	1.126
03	Silty sand	352.15~352.30	0.3154	1.079
04	Fine sand	444.15~444.30	0.3674	1.080
05	Fine sand	552.00~552.35	0.2538	1.824
06	Silty sand	560.20~560.35	0.3637	0.981

Note: h is the coring depth (m), φ is the porosity, and K is the permeability coefficient, 10^{-5} m/s.

cement ratio of slurry used on site is 1.25 : 1 and 1 : 1, and the slurry with water cement ratio of 1 : 1 is mainly used. The physical parameters of the core soil sample taken from the 3rd wind inspection hole are listed in Table 1, and the grouting test results of each grouting section are listed in Table 2.

Substituting the relevant parameters from Tables 1 and 2 into Equation (56), the theoretically calculated values of the initial grouting pressure of the ZJ3, ZJ4, and ZJ5 grouting sections were 9.05 MPa, 7.31 MPa, and 5.46 MPa, respectively, and the associated errors of the initial grouting pressure values in Table 2 were -9.41%, 9.27%, and 13.75%, respectively. Substituting the relevant parameters from Tables 1 and 2 into Equation (55), the theoretically calculated values of the diffusion radius of the ZJ3 to ZJ5 grouting sections were 6.57 m, 6.35 m, and 6.84 m, respectively, and the errors of the design value were -17.88%, -20.63%, and -14.50%, respectively, which are all within the engineering acceptable range [35–37], thus verifying the rationality of the theoretical model proposed in this study.

3.2. Slurry Pressure Attenuation Law. Substituting the relevant parameters from Tables 1 and 2 into Equation (57), the slurry pressure distribution curves in the diffusion zone of the ZJ3 to ZJ5 grouting sections were obtained, as shown in Figure 5. The attenuation of the slurry pressure has distinguishable stages, which decrease sharply near the grouting tube and gradually away from the grouting tube. We calculated the slurry pressure value, pressure attenuation value, and attenuation percentage at different diffusion distances, where the calculation results are listed in Table 3. At a diffusion distance of 1 m, the slurry pressure attenuation of the ZJ3 to ZJ5 grouting sections were 60.32%, 60.52%, and 51.67% of the total pressure attenuation within the diffusion range, respectively. At a diffusion distance of 2 m, the slurry pressure attenuation of the ZJ3 to ZJ5 grouting sections were 74.51%, 74.89%, and 68.61% of the total pressure attenuation within the diffusion range, respectively. Beyond a diffusion distance of 2 m, the attenuation rate of the slurry pressure slows down, which is approximately a low-speed linear attenuation. Within the first 30% of the diffusion radius, the slurry pressure decreases sharply by approximately 70%; within the last 70% of the diffusion radius, the slurry pressure decreases gradually to the remaining 30%. This relationship is consistent with the engineering practices and trends of the measured data within the relevant literature [38–40]. The reason for this is that there is a high velocity of the slurry in the area close to the grouting tube, and a lower velocity of the slurry in the area far away from the grouting tube. According to Equation (32), the slurry pressure gradient is linearly and positively correlated with the slurry velocity;

Table 2: Grouting test results of the 3rd wind inspection hole.

Grouting section no.	H (m)	t (h)	p_0 (MPa)	Q (m^3)	R (m)	Diffusion radius calculation error (%)
ZJ5	175.05~196.11	31.30	4.24~4.80	290	6.83	-14.63
ZJ4	247.34~282.00	26.40	4.89~6.69	220	6.34	-20.75
ZJ3	332.27~364.27	23.50	7.18~9.99	206	6.57	-17.88
ZJ2	430.33~462.43	22.40	8.73~13.40	140	—	—
ZJ1	540.46~574.90	20.50	11.82~13.92	166	—	—

Note: H is the depth of the grouting section, t is the grouting time, p_0 is the injection point pressure, Q is the grouting amount, and R is the theoretically calculated value of the diffusion radius. Owing to the first grouting in the ZJ1 grouting section, the grouting was stopped when only 166 m^3 of slurry was injected, and the grouting in the ZJ2 grouting section was stopped when only 140 m^3 of slurry was injected, owing to the slurry leakage from the stop-grouting plug.

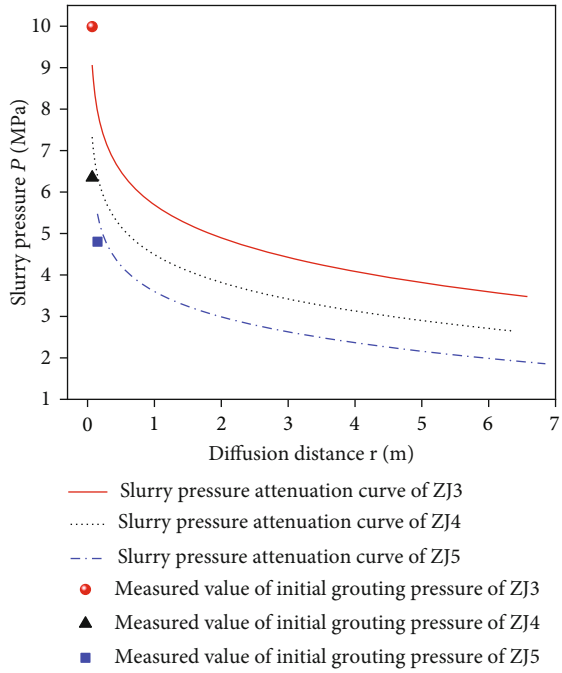

Figure 5: Pressure attenuation law of slurry.

Table 3: Slurry pressure attenuation.

Parameters	Grouting section	0	1 m	2 m	R
$P(r)$ (MPa)	ZJ3	9.05	5.69	4.90	3.48
	ZJ4	7.31	4.49	3.82	2.65
	ZJ5	5.46	3.60	2.99	1.86
$\tilde{p}(r)$ (MPa)	ZJ3	0	3.36	4.15	5.57
	ZJ4	0	2.82	3.49	4.66
	ZJ5	0	1.86	2.47	3.60
$\tilde{p}(r)/p_0 - p_w$ (%)	ZJ3	0	60.32	74.51	100
	ZJ4	0	60.52	74.89	100
	ZJ5	0	51.67	68.61	100

so, the pressure gradient decreases gradually along the diffusion direction; specifically, and the pressure decreases more slowly.

3.3. Analysis of Influencing Factors on the Diffusion Radius. When considering the field grouting parameters of the Guotun coal mine combined with Equation (55), the effects of grouting volume, grouting section height, and comprehensive layer injection rate on the grouting diffusion radius are discussed. The comprehensive layer injection rates were 0.05, 0.06, 0.07, 0.08, and 0.09, the grouting volume was 200 m^3, 250 m^3, 300 m^3, 350 m^3, and 400 m^3, and the heights of the grouting sections were 20 m, 25 m, 30 m, 35 m, and 40 m.

When the grouting section height is taken to be 30 m, the influence of the grouting volume and the comprehensive layer injection rate on the slurry diffusion radius was studied, as shown in Figure 6(a). When the comprehensive layer injection rate is taken to be 0.07, the influence of the grouting volume and grouting section height on the slurry diffusion radius is studied, as shown in Figure 6(b). When the grouting volume was 300 m^3, the influence of the grouting section height and comprehensive layer injection rate on the slurry diffusion radius was studied, as shown in Figure 6(c).

As can be seen from Figures 6(a) and 6(b), when the same grouting section height and comprehensive layer injection rate are considered, the diffusion radius increases with an increasing grouting volume, but the growth range gradually decreases. The possibility of improving the slurry diffusion radius solely by increasing the grouting volume gradually decreases. According to Figures 6(a)–6(c), the diffusion radius has a nonlinear negative correlation with the grouting section height and the comprehensive layer injection rate, the rate of change is relatively slow, and there are no distinguishable stages. Under the condition of the same grouting volume and grouting section height, it was found that increasing the comprehensive layer injection rate reduces the diffusion radius, while the grouting volume in the unit volume soil layer increases, which can effectively improve the mechanical properties of the injected layer. In engineering, multiple grouting parameters are usually coordinated and controlled to achieve the designed diffusion radius and reinforcement strength. For example, before formal grouting on site, water injection tests are often carried out to increase the hydraulic permeability of the layer, which can improve the comprehensive layer injection rate. Accordingly, the design grouting

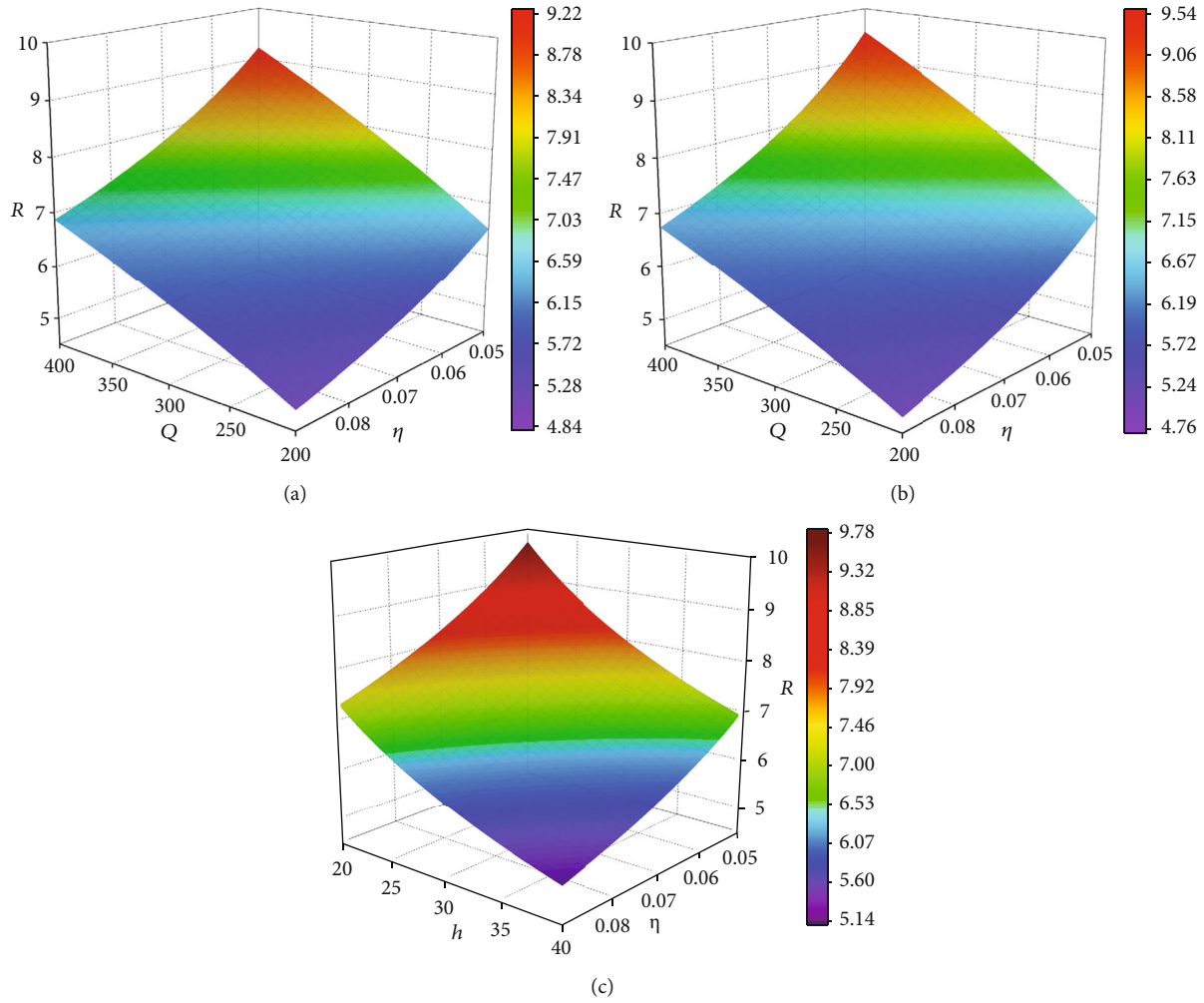

Figure 6: Analysis of the influencing factors of the grouting diffusion radius. (a) $R - Q - \eta$ 3D function image. (b) $R - Q - h$ 3D function image. (c) $R - h - \eta$ 3D function image.

volume should also be increased to achieve the desired grouting diffusion radius.

4. Conclusions

(1) The cylindrical diffusion of grouting in the deep, loose layer is regarded as the flow diffusion of slurry in a certain number of tortuous circular tubes radiated by the slurry column. The cylindrical diffusion model of the radial tube flow in a deep, loose layer is established, and the variation laws of key parameters such as slurry pressure and diffusion radius in the process of grouting are realized

(2) The permeability coefficient considering tortuosity is derived, and the average radius of the seepage tubes in the injected layer is equivalently replaced by the permeability coefficient. The diffusion velocity approximate control differential equation of the Bingham slurry in a single tube, the diffusion velocity control equation of the radiation tube flow, and the slurry pressure distribution function in the diffusion area are obtained

(3) By combining the model results with the field grouting test results in the Guotun coal mine, the rationality of the cylindrical diffusion model of radial tube flow was verified, and the attenuation law of the grouting pressure in the diffusion area is obtained. It was found that the attenuation of the slurry pressure exhibits distinguishable stages. Within the first 30% of the diffusion radius, the slurry pressure decreases sharply by approximately 70%; within the last 70% of the diffusion radius, the slurry pressure decreases gradually to the remaining 30%

(4) The calculation formula of the grouting diffusion radius is deduced, and the effects of the grouting volume, grouting section height, and comprehensive layer injection rate on the grouting diffusion radius are discussed. It is found that the diffusion radius

has a nonlinear positive correlation with the grouting volume, but the corresponding growth range gradually decreases. The diffusion radius has a nonlinear negative correlation with the grouting section height and the comprehensive layer injection rate; the rate of change is relatively low, and no distinguishable stages are observed

Data Availability

The data used to support the findings of this study are available from the corresponding author upon request.

Conflicts of Interest

The authors declare that there are no conflicts of interest regarding the publication of this paper.

Acknowledgments

The authors gratefully acknowledge the financial support of the National Natural Science Foundation of China (No. 51874005, No. 51674006, No. 51878005).

References

[1] P. Li, Q. S. Zhang, S. C. Li, and X. Zhang, "Time-dependent empirical model for fracture propagation in soil grouting," *Tunnelling and Underground Space Technology*, vol. 94, p. 103130, 2019.

[2] A. T. C. Goh, "Deterministic and reliability assessment of basal heave stability for braced excavations with jet grout base slab," *Engineering Geology*, vol. 218, pp. 63–69, 2017.

[3] A. Sohrabi-Bidar, A. Rastegar-Nia, and A. Zolfaghari, "Estimation of the grout take using empirical relationships (case study: Bakhtiari dam site)," *Bulletin of Engineering Geology and the Environment*, vol. 75, no. 2, pp. 425–438, 2016.

[4] B. Ren, W. Mu, B. Jiang et al., "Grouting mechanism in water-bearing fractured rock based on two-phase flow," *Geofluids*, vol. 2021, Article ID 5585288, 18 pages, 2021.

[5] P. Li, Q. Zhang, X. Zhang, S. Li, X. Li, and J. Zuo, "Grouting diffusion characteristics in faults considering the interaction of multiple grouting," *International Journal of Geomechanics*, vol. 17, no. 5, p. 04016117, 2017.

[6] G. Zhu, Q. Zhang, R. Liu, J. Bai, W. Li, and X. Feng, "Experimental and numerical study on the permeation grouting diffusion mechanism considering filtration effects," *Geofluids*, vol. 2021, Article ID 6613990, 11 pages, 2021.

[7] X. Du, H. Fang, S. Wang, B. Xue, and F. Wang, "Experimental and practical investigation of the sealing efficiency of cement grouting in tortuous fractures with flowing water," *Tunnelling and Underground Space Technology*, vol. 108, p. 103693, 2021.

[8] X. Liu, H. Cheng, J. Lin, C. Rong, M. Li, and H. Xu, "Study of the mechanism of fracture grouting in deeply buried rock strata based on Bingham fluid slurry," *Advances in Civil Engineering*, vol. 2019, Article ID 6943239, 10 pages, 2019.

[9] H. Cheng, X. Liu, J. Lin, L. Zhang, M. Li, and C. Rong, "Study on fracturing and diffusion mechanism of nonslab fracturing grouting," *Geofluids*, vol. 2020, Article ID 8838135, 9 pages, 2020.

[10] W. Mu, L. Li, T. Yang, G. Yu, and Y. Han, "Numerical investigation on a grouting mechanism with slurry-rock coupling and shear displacement in a single rough fracture," *Bulletin of Engineering Geology and the Environment*, vol. 78, no. 8, pp. 6159–6177, 2019.

[11] Z. Zhao, T. Wang, and X. Jin, "Study on permeation grouting rules for loess and method for predicting migration radius," *KSCE Journal of Civil Engineering*, vol. 25, no. 8, pp. 2876–2883, 2021.

[12] G. N. Karahan and O. Sivrikaya, "Designing singular jet grouting column for sandy soils," *Environmental Earth Sciences*, vol. 77, no. 12, pp. 1–11, 2018.

[13] Y. Fu, X. Wang, S. Zhang, and Y. Yang, "Modelling of permeation grouting considering grout self-gravity effect: theoretical and experimental study," *Advances in Materials Science and Engineering*, vol. 2019, Article ID 7968240, 16 pages, 2019.

[14] K. Fang, T. Zhao, Y. Tan, and Y. Qiu, "Prediction of grouting penetration height along the shaft of base grouted pile," *Journal of Marine Science and Engineering*, vol. 7, no. 7, p. 212, 2019.

[15] J. Yun, J. Park, Y. Kwon, B. Kim, and I. Lee, "Cement-based fracture grouting phenomenon of weathered granite soil," *KSCE Journal of Civil Engineering*, vol. 21, no. 1, pp. 232–242, 2017.

[16] N. Shrivastava and K. Zen, "Finite element modeling of compaction grouting on its densification and confining aspects," *Geotechnical and Geological Engineering*, vol. 36, no. 4, pp. 2365–2378, 2018.

[17] Z. Wang, J. Zou, and H. Yang, "A new approach for the fracture grouting pressure in soil mass," *Advances in Mechanical Engineering*, vol. 10, 2018.

[18] Z. Zhou, X. Du, Z. Chen, Y. Zhao, and L. Chen, "Grout dispersion considering effect of pore tortuosity," *The Chinese Journal of Nonferrous Metals*, vol. 26, no. 8, pp. 1721–1727, 2016.

[19] Q. Zhang, H. Wang, R. Liu et al., "Infiltration grouting mechanism of porous media considering diffusion paths of grout," *Chinese Journal of Geotechnical Engineering*, vol. 40, no. 5, pp. 918–924, 2018.

[20] X. Chen and C. Yuan, "Law of columnar penetration of Bingham type slurry in porous media," *Journal of Mining and Safety Engineering*, vol. 38, no. 4, pp. 800–809, 2021.

[21] J. Liu, Q. Zhang, L. Zhang, F. Peng, Z. Li, and X. Weng, "Model test on segmental grouting diffusion process in muddy fault of tunnel engineering," *Geofluids*, vol. 2020, 12 pages, 2020.

[22] B. Ren, L. Wang, H. Fan, K. Ding, K. Wang, and C. Jiang, "Unsteady approximate model of grouting in fractured channels based on Bingham fluid," *Geofluids*, vol. 2021, Article ID 6671982, 13 pages, 2021.

[23] J. Liu, K. Yuen, W. Chen, X. Zhou, and W. Wang, "Grouting for water and mud inrush control in weathered granite tunnel: a case study," *Engineering Geology*, vol. 279, p. 105896, 2020.

[24] X. Huang, Z. Yao, H. Cai, X. Li, and H. Chen, "Performance evaluation of coaxial borehole heat exchangers considering ground non-uniformity based on analytical solutions," *International Journal of Thermal Sciences*, vol. 170, p. 107162, 2021.

[25] R. T. Grotenhuis, *Fracture Grouting in Theory: Modelling of Fracture Grouting in Sand*, Delft University of Technology, Delft, 2004.

[26] A. Bezuijen, R. T. Grotenhuis, A. F. V. Tol, J. W. Bosch, and J. K. Haasnoot, "Analytical model for fracture grouting in

sand," *Journal of Geotechnical and Geoenvironmental Engineering*, vol. 137, no. 6, pp. 611–620, 2011.

[27] S. Wang, B. Yu, Q. Zheng, Y. Duan, and Q. Fang, "A fractal model for the starting pressure gradient for Bingham fluids in porous media embedded with randomly distributed fractal-like tree networks," *Advances in Water Resources*, vol. 34, no. 12, pp. 1574–1580, 2011.

[28] X. Y. Kong, *Advanced Seepage Mechanics*, China University of Science and Technology Press, Hefei, 2020.

[29] E. A. Saied and M. E. Khalifa, "Some analytical solutions for groundwater flow and transport equation," *Transport in Porous Media*, vol. 47, no. 3, pp. 295–308, 2002.

[30] P. K. Kundu, I. M. Cohen, and D . Dowling, *Fluid Mechanics*, American Academic Press, Waltham, 2016.

[31] C. Li and X. Zhang, "Unification of flow equations in tubes and in porous media," *Xinjiang Petroleum Geology*, vol. 28, no. 2, pp. 252-253, 2007.

[32] L. Chen, Q. Kang, R. Pawar, Y. He, and W. Tao, "Pore-scale prediction of transport properties in reconstructed nanostructures of organic matter in shales," *Fuel*, vol. 158, pp. 650–658, 2015.

[33] D. Fan and A. Ettehadtavakkol, "Analytical model of gas transport in heterogeneous hydraulically-fractured organic-rich shale media," *Fuel*, vol. 207, pp. 625–640, 2017.

[34] M. Chang and R. Huang, "Observations of hydraulic fracturing in soils through field testing and numerical simulations," *Canadian Geotechnical Journal*, vol. 53, no. 2, pp. 343–359, 2016.

[35] J. I. Adachi and E. Detournay, "Plane strain propagation of a hydraulic fracture in a permeable rock," *Engineering Fracture Mechanics*, vol. 75, no. 16, pp. 4666–4694, 2008.

[36] Q. Zhang, L. Zhang, R. Liu, S. Li, and Q. Zhang, "Grouting mechanism of quick setting slurry in rock fissure with consideration of viscosity variation with space," *Tunnelling and Underground Space Technology*, vol. 70, pp. 262–273, 2017.

[37] Z. Zhang, H. Xie, R. Zhang et al., "Deformation damage and energy evolution characteristics of coal at different depths," *Rock Mechanics and Rock Engineering*, vol. 52, no. 5, pp. 1491–1503, 2019.

[38] B. Xue, X. Du, J. Wang, and X. Yu, "A scaled boundary finite-element method with B-differentiable equations for 3D frictional contact problems," *Fractal and Fractional*, vol. 6, no. 3, p. 133, 2022.

[39] Z. Wang, S. Shen, C. Ho, and Y. Kim, "Investigation of field-installation effects of horizontal twin-jet grouting in Shanghai soft soil deposits," *Canadian Geotechnical Journal*, vol. 50, no. 3, pp. 288–297, 2013.

[40] L. P. Chegbeleh, T. M. Akabzaa, J. A. Akudago, and S. M. Yidana, "Investigation of critical hydraulic gradient and its application to the design and construction of bentonite-grout curtain," *Environmental Earth Sciences*, vol. 78, no. 12, 2019.